



Benzimidazole-based imine-linked chemosensor: chromogenic sensor for Mg^{2+} and fluorescent sensor for Cr^{3+}

Preeti Saluja^a, Hemant Sharma^a, Navneet Kaur^b, Narinder Singh^{a,*}, Doo Ok Jang^{c,*}

^a Department of Chemistry, Indian Institute of Technology Ropar, Rupnagar, Punjab 140001, India

^b Centre for Nanoscience & Nanotechnology, Punjab University, Chandigarh, Punjab 160014, India

^c Department of Chemistry, Yonsei University, Wonju, Gangwon 220-710, Republic of Korea

ARTICLE INFO

Article history:

Received 16 December 2011

Received in revised form 16 January 2012

Accepted 17 January 2012

Available online 24 January 2012

Keywords:

Multifunctional sensor

Benzimidazole

Chemosensor

$Mg(II)$

$Cr(III)$

ABSTRACT

We synthesized an imine-linked, benzimidazole-based chemosensor that can be used for chromogenic recognition of Mg^{2+} and fluorescent recognition of Cr^{3+} . The chemosensor shows sensitive, selective, and ratiometric recognition of Cr^{3+} through concurrent quenching at one wavelength and enhancement of fluorescence intensity at another wavelength. It can also be used to detect Mg^{2+} via UV–vis absorption spectroscopy. DFT calculations support these phenomena. The sensor can be used to strain microbe cells without breakage.

© 2012 Elsevier Ltd. All rights reserved.

1. Introduction

Sugar-laden food, high calorie intake, and a sedentary lifestyle increase the risk of diabetes. Recent studies have shown that deficiency in two trace minerals, i.e., magnesium and chromium, is also responsible for type 2 diabetes.¹ Chromium improves insulin sensitivity and acts as a glucose tolerance factor through the metabolism of carbohydrates, fats, and protein.² Magnesium is a co-factor in the phosphorylation of glucose during carbohydrate metabolism.³ In addition, Mg^{2+} is also required for the proper functioning of the nerves and the immune system and for muscle and bone health.⁴ Mg^{2+} and Cr^{3+} represent an interesting paradox in the human body as a trace amount of both is required for normal physiological functions. However, unregulated amounts of both may cause serious problems.⁵ Magnesium may lead to hypermagnesemia⁶ and chromium interacts with some medications such as beta-blockers and NSAIDs.⁷ Hence, measuring Mg^{2+} and Cr^{3+} in the blood serum is a necessary component of epidemiologic studies,⁸ and the estimation of these minerals in food stuffs may help to formulate guidelines for determining the dietary requirements of diabetic patients.

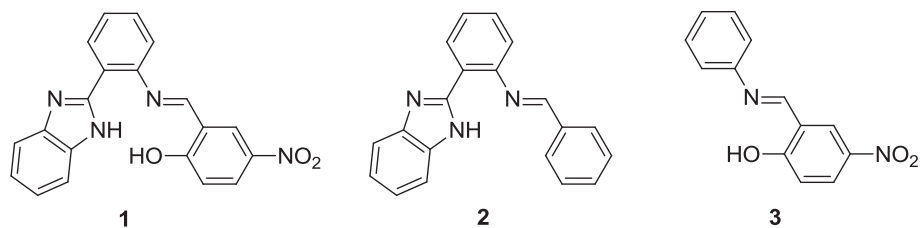
These facts encouraged us to develop a sensor for the estimation of both Mg^{2+} and Cr^{3+} under biological conditions. In continuation

of our ongoing research for the development of multifunctional sensors,⁹ here we report a sensor comprised of two dyes that was fabricated in such a way that one dye has hard binding sites for Mg^{2+} and the other dye contains borderline binding sites for Cr^{3+} . These two dyes respond differently when probed by two different spectroscopic techniques. Such multifunctional sensors have many advantages: (a) the sensor is devised for two metal ions, and if the concentration of these metal ions is estimated through two different techniques, then this will avoid interference in estimation; (b) this strategy is useful where a large amount of sample is not available for individual estimation of both analytes; (c) this method is less time consuming as the analyst has to prepare only a single sample for analysis of both metal ions.

2. Results and Discussion

We synthesized sensor **1** by a simple condensation reaction between 2-(2-aminophenyl)-1*H*-benzimidazole (fluorescent moiety) and 2-hydroxy-5-nitrobenzaldehyde (chromogenic moiety). Sensor **1** is designed based upon recognition studies of sensors **2** and **3**, which were synthesized via a condensation reaction (Scheme 1).¹⁰ Sensor **2** was found to be a fluorescent sensor for Cr^{3+} and this binding event led to quenching in intensity at 425 nm and a small enhancement at 480 nm in a HEPES buffered CH_3CN/H_2O (8:2, v/v, pH=7.0) solvent system (Figs. S4A and S5). However, sensor **2** was not selective for Cr^{3+} and also showed some affinity

* Corresponding authors. E-mail addresses: nsingh@iitrpr.ac.in (N. Singh), dojang@yonsei.ac.kr (D.O. Jang).



Scheme 1.

for other metal ions. Similarly, sensor **2** was not selective for any particular metal ion when the metal binding affinity of **2** was tested with UV–vis absorption spectroscopy (Fig. S4B). Sensor **3** had some affinity for Mg^{2+} as evident from the changes in the UV–vis spectra of **3** when recorded in a HEPES buffered CH_3CN/H_2O (8:2, v/v, pH=7.0) solvent system (Fig. S6A). The successive addition of Mg^{2+} to a solution of **3** resulted in an increase in absorbance at 355 nm and a decrease in absorbance at 395 nm with two isosbestic points at 385 and 450 nm (Fig. S7). However, sensor **3** is limited by the fact that further addition of Mg^{2+} led to some precipitation. The fluorescence spectra of **3** were not shifted selectively for any particular metal ion (Fig. S6B). Binding sites of sensors **2** and **3** provided a sufficient background for sensor design, which can be used for the simultaneous estimation of Mg^{2+} and Cr^{3+} .

The UV–vis spectrum of sensor **1** was recorded in a HEPES buffered CH_3CN/H_2O (8:2, v/v, pH=7.0) solvent system. The absorption spectrum of sensor **1** displayed well-defined bands at 300, 350, and 400 nm. The role of pH on the photophysical properties of sensor **1** was evaluated by varying the pH of the solution from 1.3 to 13.1. The acidic pH range drastically affected the photophysical properties of sensor **1** as evident in Fig. S8. Therefore, to preclude the influence of pH, all the studies were carried out in a HEPES buffered solution (pH=7.0±0.1). The cation binding affinity of sensor **1** toward different alkali, alkaline earth, and transition metal ions was investigated with fluorescence and UV–vis absorption spectroscopy. Upon addition of Mg^{2+} to a solution of sensor **1** in HEPES buffered CH_3CN/H_2O (8:2, v/v, pH=7.0), the observed absorption band of sensor **1** at 400 nm decreased in absorbance and the other two bands showed an increase in absorbance (Fig. 1A). However, no such significant changes in sensor **1** were observed with any other tested cations. To gain more insight into the photophysical properties of sensor **1** as a chromogenic sensor for Mg^{2+} , a titration was performed (Fig. 1B). Successive additions of Mg^{2+} to a solution of sensor **1** in HEPES buffered CH_3CN/H_2O (8:2, v/v, pH=7.0) led to a stepwise decrease in absorbance at 400 nm and an increase in absorbance at 350 nm with a clear isosbestic point at 385 nm. The preferential binding of Mg^{2+} in the pseudocavity of sensor **1** reveals that the sensor binding sites are complementary to Mg^{2+} in terms of size and hard–hard interactions. The detection range was turned out to be 3.2–100 μM .

The stoichiometry of the **1**· Mg^{2+} complex was determined by mass spectrometry and the Job plot method.¹¹ The mass spectrum of **1**· Mg^{2+} revealed a 1:1 stoichiometry of the complex based on the presence of a peak at $m/z=382$ (Fig. S9). The Job plot analysis indicated the formation of a 1:1 host/guest complex (Fig. S12). A K_a value of **1**· Mg^{2+} was calculated based on the UV–vis absorption titration¹² and was found to be $3.2(\pm 0.1) \times 10^2 M^{-2}$.

Cr^{3+} binding with sensor **1** led to a change in the fluorescent spectra of **1** with quenching at 415 nm and enhancement at 475 nm. No such significant and unique changes were observed upon binding of any of the other metal ions (Fig. 2A). To evaluate sensor **1** as a fluorescent sensor for Cr^{3+} , titrations were performed with successive additions of Cr^{3+} to a solution of **1** in HEPES buffered CH_3CN/H_2O (8:2, v/v, pH=7.0), which led to the same type of profile as observed in Fig. 2A, i.e., quenching in the fluorescence

intensity of **1** at 415 nm and enhancement at 475 nm (Fig. 2B). Such changes at two wavelengths offer an interesting opportunity for ratiometric fluorescence determination of analytes (Fig. S14). Ratiometric determinations have advantages over conventional monitoring at a single wavelength because the system is free from errors, which cause sensor concentrations, photo-bleaching, and so on.¹³ The stoichiometry of the complex was determined with mass spectra, showing the formation of a 2:1 host/guest complex based on the presence of a peak at $m/z=768$ (Fig. S10). The Job plot analysis for the complex formed between **1** and Cr^{3+} was at maximum at a molar fraction of Cr^{3+} at 0.66, also confirming the formation of a 2:1 host/guest complex for Cr^{3+} (Fig. S13). The association constant for **1**· Cr^{3+} was calculated by fluorescence titration, and was found to be $1.6(\pm 0.1) \times 10^4 M^{-2}$. The detection range was turned out to be 79.4–340 μM .

The complementary relationship between host and guest was further confirmed with density functional theory (DFT) calculations using Becke's three parameterized Lee–Yang–Parr (B3LYP) exchange functional with 6-31G* basis sets on Gaussian 09

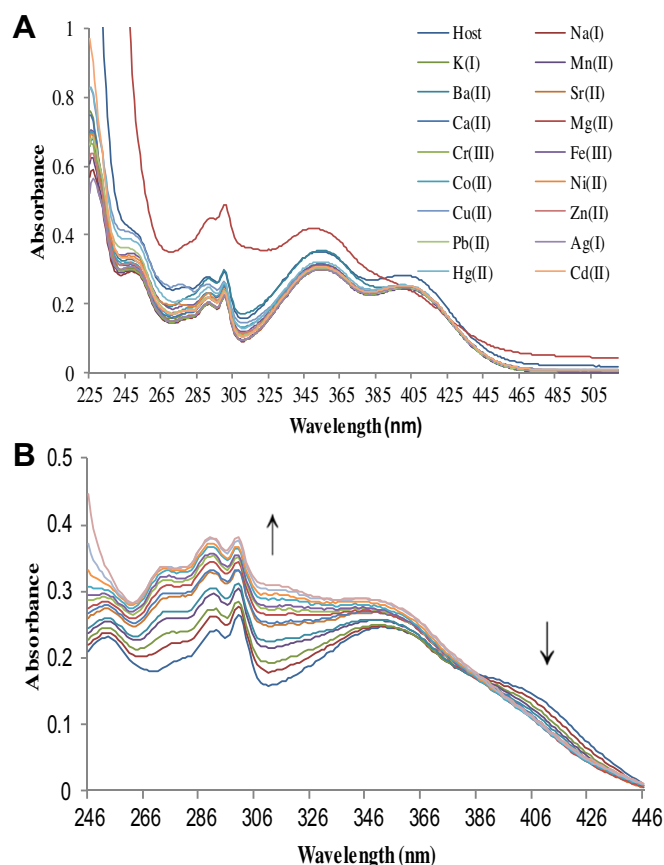


Fig. 1. (A) Changes in the UV–vis absorption spectra of sensor **1** (1.5 μM) in the presence of metal nitrate salts in HEPES buffered CH_3CN/H_2O (8:2, v/v, pH=7.0). (B) Changes in UV–vis absorption spectra of sensor **1** (1.5 μM) with increasing concentrations of Mg^{2+} in HEPES buffered CH_3CN/H_2O (8:2, v/v, pH=7.0).

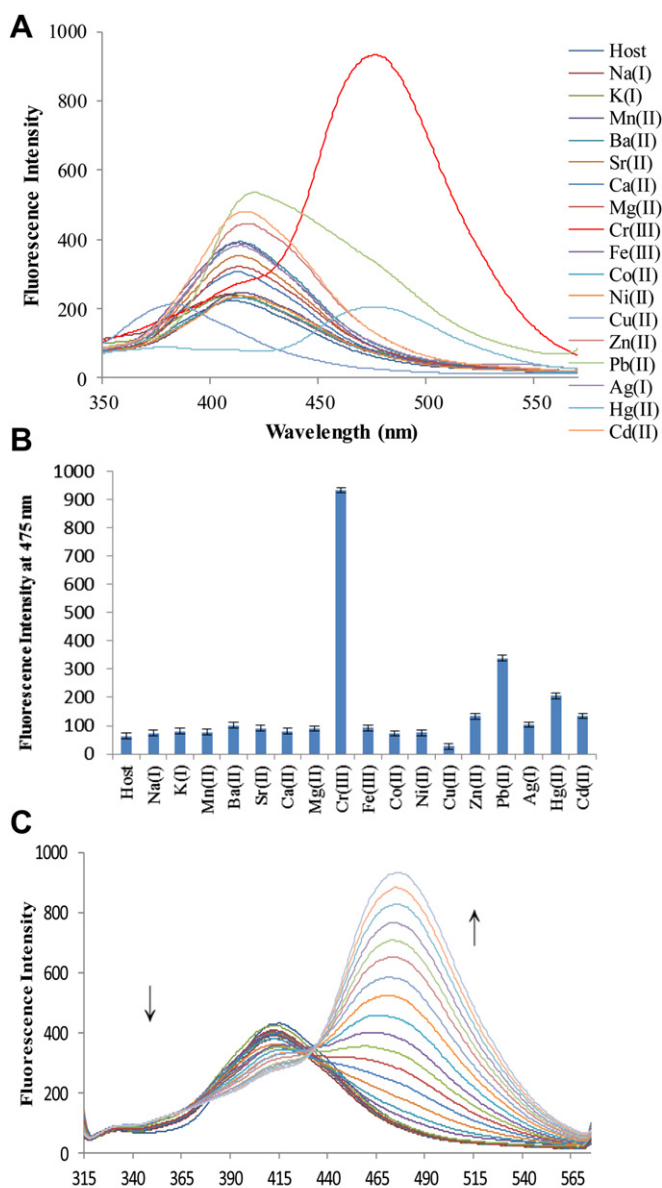


Fig. 2. (A) Changes in the fluorescence spectrum of **1** (0.5 μ M) upon addition of metal nitrate salts in HEPES buffered $\text{CH}_3\text{CN}/\text{H}_2\text{O}$ (8:2, v/v, pH=7.0) with excitation at 300 nm. (B) A bar diagram showing fluorescence intensity in the presence of different metals at 475 nm. (C) Changes in the fluorescence spectrum of sensor **1** (0.5 μ M) with increasing concentrations of Cr^{3+} in HEPES buffered $\text{CH}_3\text{CN}/\text{H}_2\text{O}$ (8:2, v/v, pH=7.0).

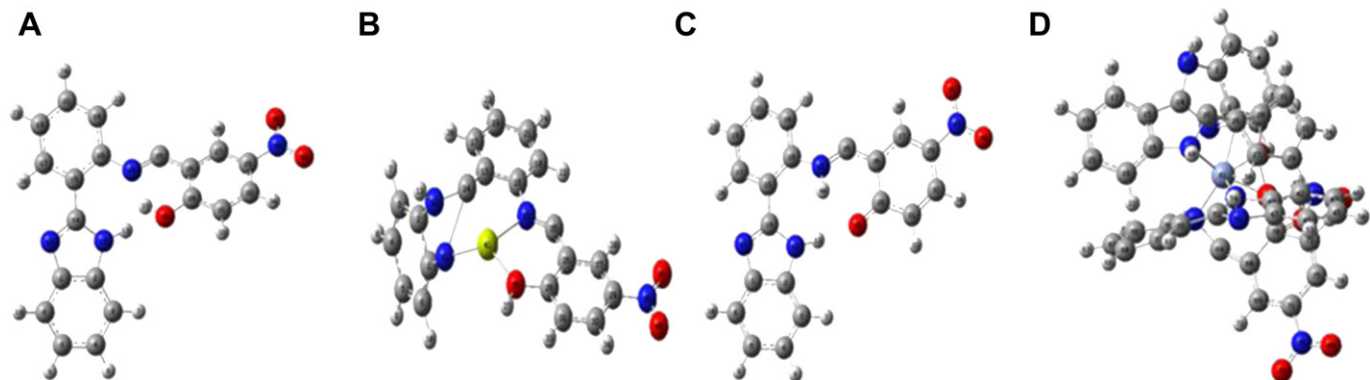


Fig. 3. Optimized structure of (A) the enol form of **1**, (B) the Mg^{2+} complex with the enol form of **1**, (C) the keto form of **1**, and (D) the Cr^{3+} complex with the keto form of **1**. Red, blue and gray spheres correspond to O, N, and C atoms, respectively, while yellow and sky-blue spheres are Mg^{2+} and Cr^{3+} , respectively. The labeling of each atom is shown in Fig. S15. DFT calculations were performed with the B3LYP exchange functional with a 6-31G* base set using a suite of Gaussian 09 programs.

programs.¹⁴ The optimized structure of the enol form of sensor **1** and its Mg^{2+} complex are shown in Fig. 3A and B. The enol form of **1** has symmetry with three different planes that intersect each other, shown by dihedral angles in Table S1. However, a Mg^{2+} complex with the enol form of **1** results in marked changes in the geometry of **1** upon coordination with Mg^{2+} . A comparison of the optimized structures of **1** and the $\mathbf{1}\cdot\text{Mg}^{2+}$ complex reveals that the face of the benzimidazole moiety rotates to provide a binding site for Mg^{2+} , i.e., N11 and N12 exchange their positions during formation of the complex. This event leads to the destruction of intramolecular hydrogen bonding in the complex, which prevails in **1**. However, the metal complex is more stable than the enol form of **1** as evident from the comparison of total energy of the enol form of **1** and its Mg^{2+} complex (Table S2).

The modulation of the fluorescence spectrum of **1** with the addition of Cr^{3+} is due to the formation of a more stable Cr^{3+} complex with the keto form of **1**, which occurs due to the excited state intramolecular proton transfer (ESIPT) from the enol form of **1** through keto–enol tautomerism. In the absence of Cr^{3+} , the enol form is in equilibrium with its keto tautomer in the excited state. As Cr^{3+} binds to the keto form, the keto form is removed from equilibrium, which is maintained via the production of more keto tautomer. Thus, the intensity due to the enol tautomer decreases while that from the Cr^{3+} -bound keto tautomer increases.

The DFT calculations for keto and enol forms are shown in Fig. 3A and C. C_1 symmetry of the enol form of **1** having aromatic moieties in three different planes approaches planarity in the keto form of **1**, as supported by the dihedral angles shown in Table S1. This concept of more planarity in the keto form is further strengthened by comparison of the bond distance between $\text{O}36\cdots\text{H}13$ in both forms of **1**, i.e., this bond distance is 3.05 Å in the enol form and that of the keto form is 1.91 Å. Due to flipping of the 2-hydroxy-5-nitro benzene moiety, O36 in the keto form comes close to N12 and N25 and forms a pseudocavity with two intramolecular hydrogen bonds as compared to the enol form, which has only one due to the non-planarity in the structure. In the keto form, the hydrogen bonding distances between $\text{O}36\cdots\text{H}13$ and $\text{O}36\cdots\text{H}40$ are found to be 1.91 Å and 1.95 Å, respectively.

The DFT calculated structure of the Cr^{3+} complex (host/guest=2:1) with the keto form of **1** has a multifaceted structure with two intramolecular hydrogen bonds, $\text{N}37\cdots\text{H}77$ and $\text{O}36\cdots\text{H}10$ with lengths of 1.99 Å and 1.42 Å, respectively. The optimized energy data indicates that the keto form of **1** with Cr^{3+} forms a more stable complex as compared to the enol complex formed with Mg^{2+} , shown in Table S2. The calculated molecular orbital diagrams from the optimization data support the shifts in

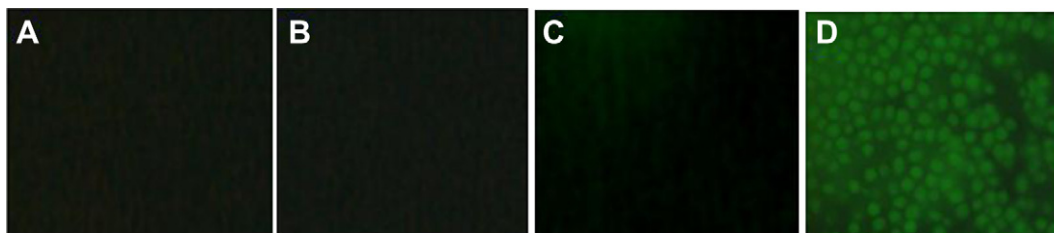


Fig. 4. Microscopic images of (A) blank yeast cells, (B) yeast cells cultured in medium enriched with Cr^{3+} , (C) blank yeast cells treated with sensor **1**, and (D) yeast cells cultured in medium enriched with Cr^{3+} and then treated with sensor **1** (before performing microscopy, the cells were washed with a $\text{CH}_3\text{CN}/\text{H}_2\text{O}$ (8:2, v/v, pH=7.0) solvent mixture).

fluorescence bands. The energy gaps between the HOMO–LUMO of the enol and keto forms of **1** and the Cr^{3+} complex with the keto form of **1** were calculated in the absence of any solvent. The energy gaps were found to be 269.9, 173.7, and 70.6 kJ/mol, respectively. These calculated values are consistent with the experimental data obtained in HEPES buffered $\text{CH}_3\text{CN}/\text{H}_2\text{O}$ (8:2, v/v, pH=7.0). That is, fluorescence emissions of the enol and keto forms of **1** and the Cr^{3+} complex with the keto form of **1** are at 415, 470, and 475 nm, respectively. Frontier molecular orbital diagrams clarify that the HOMO has high electron density in the pseudocavity region of both forms of **1**, which results in cation–dipole interactions between the metal cation and ligand (Table S3). These cation–dipole interactions give rise to stability in the $\mathbf{1}\cdot\text{Cr}^{3+}$ complex. The same coordination sphere of **1** for both of Mg^{2+} and Cr^{3+} was also confirmed with IR spectra and mass spectrometry. The IR band of **1** at 1640 cm^{-1} is assigned to $-\text{CH}=\text{N}-$ and is shifted to higher wave numbers in both complexes. Similarly, a broad IR band of **1** up to 3740 cm^{-1} due to $-\text{OH}$ is also shifted to 3690 and 3680 cm^{-1} for the Mg^{2+} and Cr^{3+} complexes, respectively.

To test the practical applicability of sensor **1** as a chromogenic sensor for Mg^{2+} as well as a fluorescence sensor for Cr^{3+} , competitive experiments were carried out. In the first set of experiments, a solution of Mg^{2+} and Cr^{3+} was added to a solution of **1**. A mass spectrum of the resulting complex showed the existence of a 1:1 complex for Mg^{2+} and a 2:1 complex for Cr^{3+} (Fig. S11). From this evidence, we conclude that the formation of complexes with both metal ions is independent of the presence of another metal ion. Further, there is no expected influence from the estimation of another metal ion (Fig. S17). Practically, a comparison of the fluorescence intensity of **1** in the presence of 1 equiv of Cr^{3+} and secondly in the presence of 1 equiv of each of Cr^{3+} and Mg^{2+} showed that estimation of Cr^{3+} was independent of the presence of Mg^{2+} . Similarly, an independent experiment also showed that the estimation of Mg^{2+} with sensor **1** using UV–vis absorption was not affected by the presence of Cr^{3+} .

To evaluate the application of sensor **1** in biological systems,¹⁵ we cultured *Saccharomyces cerevisiae* (yeast) in normal broth and under experimental media containing $\text{Mg}^{2+}/\text{Cr}^{3+}$. The cells cultured in normal media and media containing Cr^{3+} ions were treated with sensor **1** (dissolved in a HEPES buffered $\text{CH}_3\text{CN}/\text{H}_2\text{O}$ (8:2, v/v, pH=7.0) solvent mixture). Before performing microscopy, the cells were washed with a $\text{CH}_3\text{CN}/\text{H}_2\text{O}$ (8:2, v/v, pH=7.0) solvent mixture. The microscopic investigations revealed that sensor **1** is capable of binding Cr^{3+} in a cellular medium (Fig. 4). Similarly, cells were cultured to investigate the role of sensor **1** for Mg^{2+} . However, color changes due to the binding of Mg^{2+} were not so distinct under optical microscopy, although the changes in absorbance were measurable with diffuse reflectance under UV–vis absorption spectroscopy.

The microscopic image (Fig. 4D) clearly shows that sensor **1** passes through the yeast cell membrane and stains the cytoplasm enriched with Cr^{3+} . To confirm that sensor **1** does not lead to the destruction of the microbe, SEM images of the cells cultured with Cr^{3+} and then treated with sensor **1** were obtained. The smoothness of the microbe surface in both cases confirms that sensor **1** does not cause any breakage to the surface of the microbe (Fig. 5).

3. Conclusion

In conclusion, an imine-linked, benzimidazole-based chemosensor was synthesized for chromogenic recognition of Mg^{2+} and fluorescent recognition of Cr^{3+} . The chemosensor was found to provide sensitive, selective, and ratiometric recognition of Cr^{3+} through concurrent quenching at one wavelength and enhancement of fluorescence intensity at the other wavelength. The same sensor can be used to detect Mg^{2+} using UV–vis absorption spectroscopy. The results are supported with DFT calculations. The sensor is applicable for straining microbial cells without any breakage.

Acknowledgements

This work was supported by the India–Korea Joint Program of Cooperation in Science & Technology (2011–0027710) and the CSIR project (01(2417)/10/EMR-II). P.S. is thankful to UGC India for a research fellowship. We thank Mr. S. Soni of CSIO Chandigarh for fluorescence microscopy assistance.

Supplementary data

Supplementary data related to this article can be found in the online version, at doi:10.1016/j.tet.2012.01.047.

References and notes

- (a) O'Connell, B. S. *Diabetes Spectrum* **2001**, *14*, 133; (b) Elamin, A.; Tuvemo, T. *Diabetes Res. Clin. Pract.* **1990**, *10*, 203; (c) Lima, M. L.; Cruz, T.; Rodrigues, L. E.;

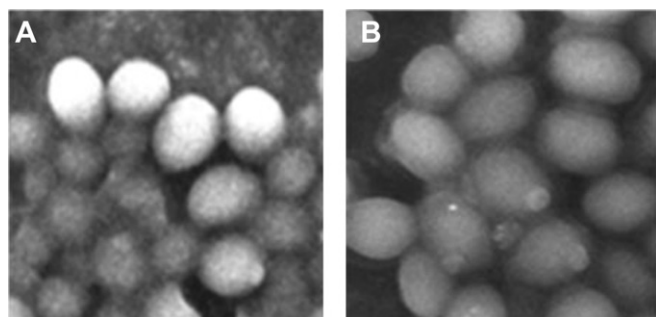


Fig. 5. SEM images showing the surface morphology of (A) normal yeast cells and (B) yeast cells cultured with Cr^{3+} and then treated with sensor **1** (before performing microscopy, the cells were washed with a $\text{CH}_3\text{CN}/\text{H}_2\text{O}$ (8:2, v/v, pH=7.0) solvent mixture).

- Bomfim, O.; Melo, J.; Correia, R.; Porto, M.; Cedro, A.; Vicente, E. *Diabetes Res. Clin. Pract.* **2009**, *83*, 257.
2. (a) Anderson, R. A. *J. Am. Coll. Nutr.* **1998**, *17*, 548; (b) Mertz, W. *Nutr. Rev.* **1998**, *56*, 174; (c) Anderson, R. A.; Cheng, N.; Bryden, N. A.; Polansky, M. M.; Chi, J.; Feng, J. *Diabetes* **1997**, *46*, 1786.
3. (a) O'Rourke, B.; Backx, P. H.; Marban, E. *Science* **1992**, *257*, 245; (b) Politi, H. C.; Preston, R. R. *Neuroreport* **2003**, *14*, 659; (c) Dai, L.-J.; Ritchie, G.; Kerstan, D.; Kang, H. S.; Cole, D. E. C.; Quamme, G. A. *Physiol. Rev.* **2001**, *81*, 51; (d) Schmitz, C.; Perraud, A.; Johnson, C. O.; Inabe, K.; Smith, M. K.; Penner, R.; Kurosaki, T.; Fleig, A.; Scharenberg, A. M. *Cell* **2003**, *113*, 191; (e) Flatman, P. W. *Annu. Rev. Physiol.* **1991**, *53*, 259; (f) Rude, G. A. *Am. J. Cardiol.* **1989**, *63*, 316; (g) Grubb, R. D.; Maguire, M. E. *Magnesium* **1987**, *6*, 113; (h) Hartwig, A. *Mutat. Res.* **2001**, *475*, 1133.
4. (a) Ajayaghosh, A.; Arunkumar, E.; Daub, J. *Angew. Chem., Int. Ed.* **2002**, *41*, 1766; (b) Ozmen, B.; Akkaya, E. U. *Tetrahedron Lett.* **2000**, *41*, 9185; (c) Kim, H. J.; Kim, J. S. *Tetrahedron Lett.* **2006**, *47*, 7051; (d) Mahabir, S.; Wei, Q. Y.; Barrera, S. L.; Dong, Y. Q.; Etzel, C. J.; Spitz, M. R.; Forman, M. R. *Carcinogenesis* **2008**, *29*, 949; (e) Nielsen, F. H.; Lukaski, H. C. *Magnes. Res.* **2006**, *19*, 180; (f) Stepura, O. B.; Martynow, A. I. *Int. J. Cardiol.* **2009**, *134*, 145; (g) Larsson, S. C.; Virtanen, M. J.; Mars, M.; Pietinen, P.; Albanes, D.; Virtamo, J. *Arch. Intern. Med.* **2008**, *168*, 459; (h) Farruggia, G.; Lotti, S.; Prodi, L.; Montalti, M.; Zaccheroni, N.; Savage, P. B.; Trapani, V.; Sale, P.; Wolf, F. J. *Am. Chem. Soc.* **2006**, *128*, 344; (i) Kar, P.; Suresh, M.; Krishnakumar, D.; Jose, D. A.; Ganguly, B.; Das, A. *Polyhedron* **2007**, *26*, 1317; (j) Gunther, T. J. *Clin. Chem. Clin. Biochem.* **1977**, *15*, 433; (k) Shine, K. I. *Am. J. Physiol.* **1979**, *237*, 413; (l) Ackerman, K. E. O.; Nicholls, D. G. *Rev. Physiol. Biochem. P.* **1983**, *95*, 149.
5. (a) Hans, C. P.; Sialy, R.; Bansal, D. D. *Curr. Sci.* **2002**, *83*, 1456; (b) Kortenkamp, A.; Casadevall, M.; Faux, S. P.; Jenner, A.; Shayer, R. O. J.; Woodbridge, N.; O'Brien, P. *Arch. Biochem. Biophys.* **1996**, *329*, 199.
6. (a) Guerrero-Romero, F.; Rodriguez-Moran, M. *Acta Diabetol.* **2002**, *39*, 209; (b) Bradford, C.; McElduff, A. *Crit. Care Resusc.* **2006**, *8*, 36.
7. (a) Roebuck, J. R., Jr.; Hla, K. M.; Chambless, L. E.; Fletcher, R. H. *Ann. Intern. Med.* **1991**, *115*, 917; (b) Abraham, A. S.; Brooks, B. A.; Eylath, U. *Metabolism* **1992**, *41*, 768; (c) Hermann, J.; Arquitt, A. *Nutr. Res.* **1994**, *14*, 671; (d) Davis, M. L.; Seaborn, C. D.; Stoecker, B. J. *Nutr. Res.* **1995**, *15*, 201; (e) Kamath, S. M.; Stoecker, B. J.; Davis-Whitenack, M. L.; Smith, M. M.; Adeleye, B. O.; Sangiah, S. J. *Nutr.* **1997**, *127*, 478.
8. (a) Sreekanth, R.; Pattabhi, V.; Rajan, S. S. *Biochem. Biophys. Res. Commun.* **2008**, *369*, 725; (b) Sharma, S.; Agrawal, R. P.; Choudhary, M.; Jain, S.; Goyal, S.; Agarwal, V. J. *Trace Elem. Med. Biol.* **2011**, *25*, 149; (c) Hunt, A. E.; Allen, K. G. D.; Smith, B. A. *Nutr. Res.* **1985**, *5*, 131.
9. (a) Lee, D. Y.; Singh, N.; Kim, M. J.; Jang, D. O. *Org. Lett.* **2011**, *13*, 3024; (b) Singh, N.; Kaur, N.; Mulrooney, R. C.; Callan, J. F. *Tetrahedron Lett.* **2008**, *49*, 6690; (c) Singh, N.; Jung, J. H.; Jang, D. O. *Tetrahedron Lett.* **2009**, *50*, 71; (d) Lee, D. Y.; Singh, N.; Jang, D. O. *Tetrahedron Lett.* **2011**, *52*, 1368; (e) Lee, D. Y.; Singh, N.; Jang, D. O. *Tetrahedron Lett.* **2010**, *51*, 1103; (f) Jung, J. H.; Singh, N.; Lee, D. Y.; Jang, D. O. *Tetrahedron Lett.* **2009**, *50*, 5555.
10. (a) Occhipinti, G.; Bjørsvik, H.-R.; Törnroos, K. W.; Jensen, V. R. *Organometallics* **2007**, *26*, 5803; (b) Jung, H. J.; Singh, N.; Jang, D. O. *Tetrahedron Lett.* **2008**, *49*, 2960.
11. Job, P. *Ann. Chim.* **1928**, *9*, 113.
12. Bourson, J.; Pouget, J.; Valeur, B. *J. Phys. Chem.* **1993**, *97*, 4552.
13. (a) Zhao, Y.-H.; Pan, H.; Fu, G.-L.; Lin, J.-M.; Zhao, C.-H. *Tetrahedron Lett.* **2011**, *52*, 3832; (b) Lee, H.; Kim, H.-J. *Tetrahedron Lett.* **2011**, *52*, 4775; (c) Helal, A.; Kim, H.-S. *Tetrahedron Lett.* **2009**, *50*, 5510.
14. (a) Becke, A. D. *J. Chem. Phys.* **1993**, *98*, 5648; (b) Lee, C.; Yang, W.; Parr, R. G. *Phys. Rev. B* **1988**, *37*, 785.
15. An example for a probe for monitoring Cr³⁺ in living cells: Huang, K.; Yang, H.; Zhou, Z.; Yu, M.; Li, F.; Gao, X.; Yi, T.; Huang, C. *Org. Lett.* **2008**, *10*, 2557.